JVI Journals.ASM.org

Upregulation of CHOP/GADD153 during Coronavirus Infectious Bronchitis Virus Infection Modulates Apoptosis by Restricting Activation of the Extracellular Signal-Regulated Kinase Pathway

Ying Liao, To Sing Fung, Mei Huang, Shou Guo Fang, Yanxin Zhong, Ding Xiang Liu

School of Biological Sciences, Nanyang Technological University, Singapore, Singapore

Induction of the unfolded protein response (UPR) is an adaptive cellular response to endoplasmic reticulum (ER) stress that allows a cell to reestablish ER homeostasis. However, under severe and persistent ER stress, prolonged UPR may activate unique pathways that lead to cell death. In this study, we investigated the activation of the protein kinase R-like ER kinase (PERK) pathway of UPR in cells infected with the coronavirus infectious bronchitis virus (IBV) and its relationship with IBV-induced apoptosis. The results showed moderate induction of PERK phosphorylation in IBV-infected cells. Meanwhile, activating transcription factor 4 (ATF4) was upregulated at the protein level in the infected cells, resulting in the induction in *trans* of the transcription factor ATF3 and the proapoptotic growth arrest and DNA damage-inducible protein GADD153. Knockdown of PERK by small interfering RNA (siRNA) suppressed the activation of GADD153 and the IBV-induced apoptosis. Interestingly, knockdown of protein kinase R (PKR) by siRNA and inhibition of the PKR kinase activity by 2-aminopurine (2-AP) also reduced the IBV-induced upregulation of GADD153 and apoptosis induction. In GADD153-knockdown cells, IBV-induced apoptosis was suppressed and virus replication inhibited, revealing a key role of GADD153 in IBV-induced cell death and virus replication. Analysis of the pathways downstream of GADD153 revealed much more activation of the extracellular signal-related kinase (ERK) pathway in GADD153-knockdown cells during IBV infection, indicating that GADD153 may modulate apoptosis through suppression of the pathway. This study provides solid evidence that induction of GADD153 by PERK and PKR plays an important regulatory role in the apoptotic process triggered by IBV infection.

The endoplasmic reticulum (ER) is the central site of cellular metabolism and protein synthesis, folding, modification, and trafficking. When excessive ER client proteins are loaded, misfolded proteins accumulate in the ER and cause ER stress. For survival, the cell will activate several signaling pathways known as the unfolded protein response (UPR) (1, 2). To date, three key sensors of UPR, the protein kinase R-like ER kinase (PERK), activating transcription factor 6 (ATF6), and inositol-requiring enzyme 1 (IRE1), have been identified (2–5). Activation of the ER stress sensors occurs sequentially, with PERK being the first, rapidly followed by ATF6, and IRE1 is activated last. Collectively, UPR attenuates the synthesis of nascent proteins, induces degradation of misfolded proteins, and enhances the ER folding capacity, thus overcoming ER stress and restoring ER homeostasis. Therefore, short-term induction of UPR helps the cell to adapt to stressful conditions and maintain viability. However, if ER stress is persistent and the damage to the ER is too great to overcome, a prolonged UPR may trigger proapoptotic pathways and lead to cell death.

During the early stages of ER stress, PERK is released from GRP78 and activated by self-phosphorylation. The activated PERK phosphorylates eIF2α at serine 51 and in *trans* stabilizes the eIF2-GDP-eIF2B complex, inhibits the pentameric guanine exchange factor eIF2B from recycling eIF2 to its active, GTP-bound form, and impairs formation of the 43S initiation complex. Protein kinase R (PKR), which is activated by double-stranded RNA (dsRNA) during virus replication, can also phosphorylate eIF2α. The phosphorylation of eIF2α results in the shutdown of global cellular protein synthesis and a reduction of the protein load in the ER (1, 6) but enhances the translation of the activating transcription factor ATF4, which in turn activates genes involved in metabolism, oxidative stress, and apoptosis (6, 7). ATF4 promotes apoptosis by stimulating the expression of the activating transcription factor ATF3 and GADD153 (also known as CHOP or C/EBP-homologous protein), which is a death-related transcription factor contributing to the transcription of genes important for cellular remediation and apoptosis (8, 9). The identified GADD153 target genes include the genes for GADD34, ER oxidoreductin 1 (ERO1α), Bcl2, tribbles-related protein 3 (TRIB3), and death receptor 5, all of which are involved in apoptosis (9–13). Apoptosis leads to the rapid disassembly of cellular structures and organelles. This process is important in eliminating cells whose survival might be harmful to the organism as a whole, thereby providing a form of defense against viral infection. Apoptosis is also considered to be responsible for the pathologies associated with virus infection (14).

Coronaviruses are enveloped viruses with structural proteins, i.e., the spike protein (S), membrane protein (M), and small envelope protein (E), embedded in the viral envelope. The envelope wraps the nucleocapsid, which consists of a single-stranded, positive-sense RNA genome of 27,000 to 32,000 nucleotides and the nucleocapsid (N) protein. Coronavirus infection of cells imposes a profound impact on the ER by loading tremendous amounts of

Received 5 March 2013 **Accepted** 6 May 2013
Published ahead of print 15 May 2013
Address correspondence to Ding Xiang Liu, dxliu@ntu.edu.sg.
Y.L. and T.S.F. contributed equally to this article.

doi:10.1128/JVI.00626-13

viral glycoproteins on the ER and modifying the ER membranes, leading to perturbation of the ER homeostasis. Furthermore, double-membrane vesicles (DMVs), the coronavirus RNA synthesis site, and virus envelopes are derived from the ER membrane (15, 16). Upon completion of the replication and assembly cycle, virions bud from the ER-Golgi intermediate compartment (17, 18). The extensive use of the ER membrane usually overloads the ER and triggers UPR, which may be deleterious to the progress of virus infection.

Infectious bronchitis virus (IBV), a chicken coronavirus, causes respiratory disease in birds. Several reports have shown that IBV infection induces caspase-dependent apoptosis at late stages of infection in cultured cells (19–21). However, signals that initiate the apoptotic program have yet to be identified. In this study, we show that activation of the eIF2α-ATF4-GADD153 pathway by IBV infection modulates stress-induced apoptosis. Both PERK and PKR were found to be involved in induction of the eIF2α-ATF4-GADD153 pathway. In IBV-infected cells, the increased phosphorylation of PERK and eIF2α at early infection stages was clearly detected, and several genes downstream of phosphorylated eIF2α, including those for ATF4, ATF3, and GADD153, were considerably induced. Knockdown of PERK and PKR by use of small interfering RNA (siRNA) reduced the expression of GADD153 and apoptosis. Knockdown of GADD153 promoted the phosphorylation of extracellular signal-regulated kinase 1/2 (ERK1/2) and reduced apoptosis. Taken together, the data in this study demonstrate that the eIF2α-ATF4-GADD153 pathway is activated by IBV infection and that upregulation of the proapoptotic protein GADD153 plays a critical role in IBV-induced apoptosis.

MATERIALS AND METHODS

Virus propagation and cell culture. The egg-adapted Beaudette strain of IBV (ATCC VR-22) adapted to Vero cells was used in this study (22). Virus stocks were prepared by infection of Vero cells with 0.1 PFU of virus per cell and incubation at 37°C for 24 h. After three rounds of freeze-thawing, cell lysates were spun down at 3,000 rpm. Aliquots of the supernatants were stored at −80°C as the virus stock. Virus titers were determined by a plaque assay with Vero cells plated in monolayers as previously described.

Inactivation of IBV was performed by subjecting the above-mentioned virus stock to 120,000 mJ/cm^2 of 254-nm short-wave UV radiation for 10 min within a CL-1000 cross-linker (UVP) (23). The inactivated virus particles retained fusion activity but had lost the replication ability. To demonstrate that IBV had been inactivated, Western blotting was used to determine the presence or absence of viral proteins in cells infected with the UV-inactivated virus.

Vero cells were maintained in Dulbecco modified Eagle medium (DMEM) supplemented with 10% fetal bovine serum and grown at 37°C in 5% CO_2. H1299 cells were maintained in RPMI 1640 with 10% fetal bovine serum.

RNA isolation and Northern blot analysis. Cells were seeded in 100-mm-diameter dishes and infected with either 2 PFU of live IBV per cell or the same amount of UV-inactivated IBV (UV-IBV). Cells were harvested at the indicated time points (0 to 28 h postinfection [hpi]). Total RNA was isolated from the cells by use of TRIzol reagent (Invitrogen) as recommended by the manufacturer. Briefly, cells were lysed in TRIzol before a one-fifth volume of chloroform was added. The mixture was then incubated for 3 min at room temperature and centrifuged at 12,000 rpm for 15 min at 4°C. The aqueous phase was then mixed with a 1:1 volume of isopropanol and incubated for 10 min at room temperature. RNA was precipitated by centrifugation at 12,000 rpm for 10 min at 4°C. The RNA pellet was washed with 70% RNase-free ethanol and dissolved in RNase-free H_2O.

Northern blot probes were obtained by reverse transcription-PCT (RT-PCR) and labeled with digoxigenin (DIG) by using a DIG labeling kit (Roche). Briefly, 2 μg of total RNA was used to perform reverse transcription using Expand reverse transcriptase (Roche). cDNAs were then subjected to PCR using appropriate primers. Primers used for human ATF4 were 5′-CCGTCCCAAACCTTACGATC-3′ (forward) and 5′-ACTATCC TCAACTAGGGGAC-3′ (reverse). Primers used for human ATF3 were 5′-GGTTAGGACTCTCCACTCAA-3′ (forward) and 5′-AGACAGTAG CCAGCGTCCTT-3′ (reverse). Primers used for human GADD153 were 5′-GATTCCAGTCAGAGCTCCCT-3′ (forward) and 5′-GTAGTGTGG CCCAAGTGGGG-3′ (reverse). Primers used for human GADD34 were 5′-CCTGAGACTCCCCTAAAGGC-3′ (forward) and 5′-GGGGGCTAA AGGTGGGTTCC-3′ (reverse).

To analyze RNA expression by Northern blotting, 30 μg of RNA from each sample preparation was separated by electrophoresis on a 1.3% agarose formaldehyde gel and visualized by using ethidium bromide staining and UV light. RNA was transferred onto a Hybond-N$^+$ membrane (Amersham Biosciences) and hybridized with DIG-labeled DNA probes overnight at 50°C. After hybridization and stringent washes, the membrane was rinsed briefly (5 min) in washing buffer and blocked in blocking buffer for 30 min, after which the membrane was incubated with DIG antibody (Roche) solution for 30 min, washed twice for 15 min each in washing buffer, and equilibrated for 3 min in detection buffer. The signal was detected with CDP-Star (Roche) according to the manufacturer's instructions.

SDS-PAGE and Western blot analysis. Cells were infected with IBV and harvested at the indicated times points. An equal number of cells was lysed with 2× SDS loading buffer in the presence of 100 mM dithiothreitol and denatured at 100°C for 5 min. Equal amounts of total cell lysates were separated by SDS-10% PAGE and transferred onto a polyvinylidene difluoride (PVDF) membrane (Stratagene). The nonspecific antibody binding sites were blocked with blocking buffer (5% fat-free milk powder in TBST buffer [20 mM Tris-HCl, pH 7.4, 150 mM NaCl, 0.1% Tween 20]) at room temperature. The membrane was then incubated with 1 μg/ml primary antibodies in blocking buffer for 1 h. Antibodies against p-PERK, total PERK, PKR, p-eIF2α (Ser51), GADD153, ERO1α, poly(ADP-ribose) polymerase (PARP), Bcl2, p-ERK1/2, ERK1/2, β-actin, and β-tubulin were purchased from Cell Signaling Technology. Antibodies against total eIF2α, ATF3, ATF4, and TRIB3 were purchased from Abcam. IBV M protein, N protein, and S protein antibodies were raised in rabbits by use of bacterial fusion proteins (24). After washing three times with TBST, the membrane was incubated with 1:2,000-diluted anti-mouse or anti-rabbit IgG antibodies conjugated with horseradish peroxidase (Dako) in blocking buffer for 1 h at room temperature. After washing three times with TBST, the polypeptides were detected with a chemiluminescence detection kit (ECL; Amersham Biosciences) according to the manufacturer's instructions.

Treatment of IBV-infected cells with 2-AP and salubrinal. The PKR inhibitor 2-aminopurine (2-AP) was purchased from Sigma and dissolved in phosphate-buffered saline (PBS)–glacial acetic acid (200:1) with heating at 65°C for 15 min. H1299 cells were infected with IBV and treated with 10 mM 2-AP after removal of the virus at 1 hpi. The same volume of PBS-glacial acetic acid (200:1) was added to another group of IBV-infected cells as a control. Cells were harvested at 0, 2, 4, 12, and 20 hpi and then subjected to SDS-PAGE and Western blotting using p-eIF2α, eIF2α, ATF4, GADD153, and IBV M protein antibodies.

The eIF2α inhibitor salubrinal was purchased from Calbiochem and dissolved in dimethyl sulfoxide (DMSO). H1299 cells were infected with IBV and treated with 20 μM salubrinal. The same volume of DMSO was added to another group of IBV-infected cells as a negative control. Cells were harvested at 0, 12, and 20 hpi and then subjected to SDS-PAGE and Western blotting using GADD153 antibody or IBV N protein antibody.

RNA interference. H1299 cells was seeded in a 6-well plate and grown to 50 to 60% confluence. siPERK, siPKR, siGADD153, and nontarget control siRNA were purchased from Ambion. Transfection of siRNA

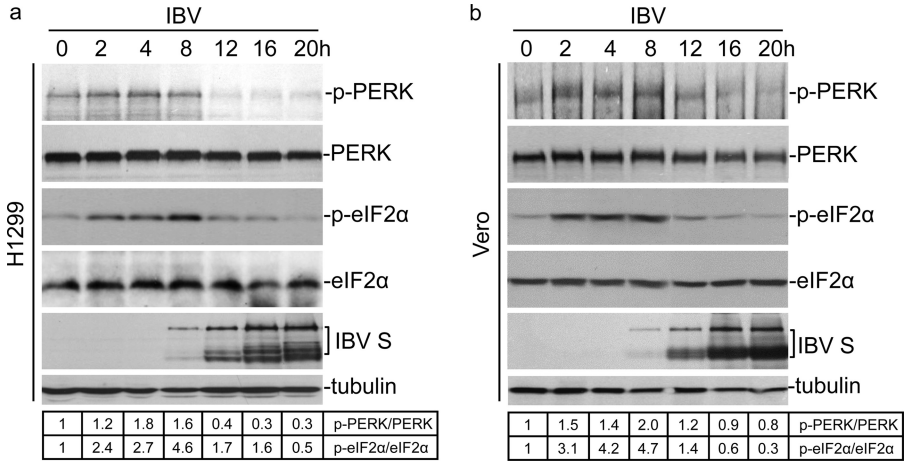

FIG 1 Phosphorylation of PERK and eIF2α in IBV-infected cells. (a) Phosphorylation of PERK and eIF2α in IBV-infected H1299 cells. H1299 cells were infected with IBV at a multiplicity of infection (MOI) of ~1 and harvested at 0, 2, 4, 8, 12, 16, and 20 hpi. Cell lysates were subjected to Western blot analysis with antibodies against phosphorylated PERK (p-PERK), total PERK, p-eIF2α, total eIF2α, and the IBV S protein. Tubulin was used as a loading control. Band intensities for p-PERK and p-eIF2α were normalized to those for total PERK and total eIF2α, respectively. The fold increases in phosphorylation are indicated below the blots, with the phosphorylation at 0 hpi given a value of 1. (b) Phosphorylation of PERK and eIF2α in IBV-infected Vero cells. Vero cells were infected as described for panel a. Western blotting and data analysis were performed as described above.

was performed using DharmaFECT 2 transfection reagent (Dharmacon, Thermo Fisher Scientific Inc.) according to the manufacturer's instructions. At 36 h posttransfection, cells were infected with IBV and harvested at the indicated time points for protein and RNA analyses.

Virus titration. Culture supernatants of infected cells were harvested and clarified by centrifugation at 13,000 rpm for 10 min at 4°C. The clarified supernatants were 10-fold serial diluted and applied to monolayers of Vero cells in 6-well plates. The plates were incubated at 37°C for 2 h, with gentle agitation every 15 min. Finally, the viruses were removed and the Vero cells were washed twice with PBS and overlaid with 0.4% agarose in DMEM. The plates were incubated at 37°C for another 2 days before being fixed with 3.7% formaldehyde in PBS. The monolayers were then stained with 0.2% crystal violet solution, and the numbers of plaques were counted. The infectious virus in each sample was titrated in triplicate, and average titers were expressed as log PFU per ml.

Densitometry. The intensities of corresponding bands were quantified using the ImageJ program (National Institutes of Health) according to the developer's instructions.

RESULTS

Upregulation of eIF2α phosphorylation by IBV infection at early stages of the infection cycle. In our previous study, phosphorylation of eIF2α was shown to be severely inhibited in IBV-infected cells at late stages of the infection cycle (25). Careful examination of both published and other unpublished data, however, showed a minimal to moderate increase of eIF2α phosphorylation at early stages of IBV infection (25). The phosphorylation status of eIF2α in IBV-infected Vero and H1299 cells was reexamined in more-detailed time course experiments, which showed a moderate increase of p-eIF2α at early time points (Fig. 1a and b). By comparing the band intensities of p-eIF2α and total eIF2α, the level of p-eIF2α was shown to increase 4.6-fold at 8 hpi and to decrease thereafter in IBV-infected H1299 cells (Fig. 1a). A significant increase of p-eIF2α was also observed in IBV-infected Vero cells (Fig. 1b). The activation of the eIF2α kinase PERK was also examined in IBV-infected Vero and H1299 cells. As shown in Fig. 1a and b, p-PERK was moderately increased at early time points in both cell lines, while total PERK was kept at a relatively steady level during the time course. These results suggest that IBV infection may activate PERK, resulting in eIF2α phosphorylation at early stages of the infection cycle.

Activation of the PERK-eIF2α-ATF4 pathway by IBV infection. Because phosphorylation of eIF2α may inhibit general protein translation but selectively promote translation of ATF4 mRNA during ER stress (7), we next asked whether the amount of phosphorylation of eIF2α observed was sufficient to induce translation of ATF4. Cell lysates prepared from IBV-infected Vero and H1299 cells were harvested at 0, 2, 4, 8, 12, 16, and 20 hpi and then subjected to Western blot analysis. Cells infected with UV-IBV were included as a control. As shown in Fig. 2a, the ATF4 protein was not detected during the early stages of infection but increased dramatically in late stages of infection, from 12 to 20 hpi in IBV-infected Vero cells and from 8 to 20 hpi in H1299 cells. ATF4 expression was not detected in cells treated with UV-IBV (Fig. 2a), indicating that ATF4 induction is due to active virus replication. The earlier detection of ATF4 in IBV-infected H1299 cells than in IBV-infected Vero cells might have been due to more active virus replication in H1299 cells. The lag between the detection of ATF4 protein expression and eIF2α phosphorylation may reflect the time required for accumulation of the ATF4 protein from a very low level to a detectable level. Northern blot analysis using an ATF4 probe showed that ATF4 induction was low to moderate at the mRNA level (Fig. 2b), confirming that the upregulation of ATF4 was due mainly to the translational enhancement.

Induction of the ATF3 gene, an ATF4 target gene (8), was examined by Northern blotting. The level of ATF3 mRNA gradually increased from 12 hpi and peaked at 28 hpi in IBV-infected Vero cells (Fig. 2c). Quantitative determination of the corresponding RNA bands showed a 33-fold induction of ATF3 in Vero cells at 28 hpi. In IBV-infected H1299 cells, ATF3 was initially decreased, at 4 and 8 hpi, but was greatly induced afterwards (Fig. 2c). At 24 and 28 hpi, less ATF3 mRNA was detected, due to massive cell death and RNA degradation (Fig. 2c). Interestingly, there were two RNA bands detected with H1299 cells, which may represent alternative

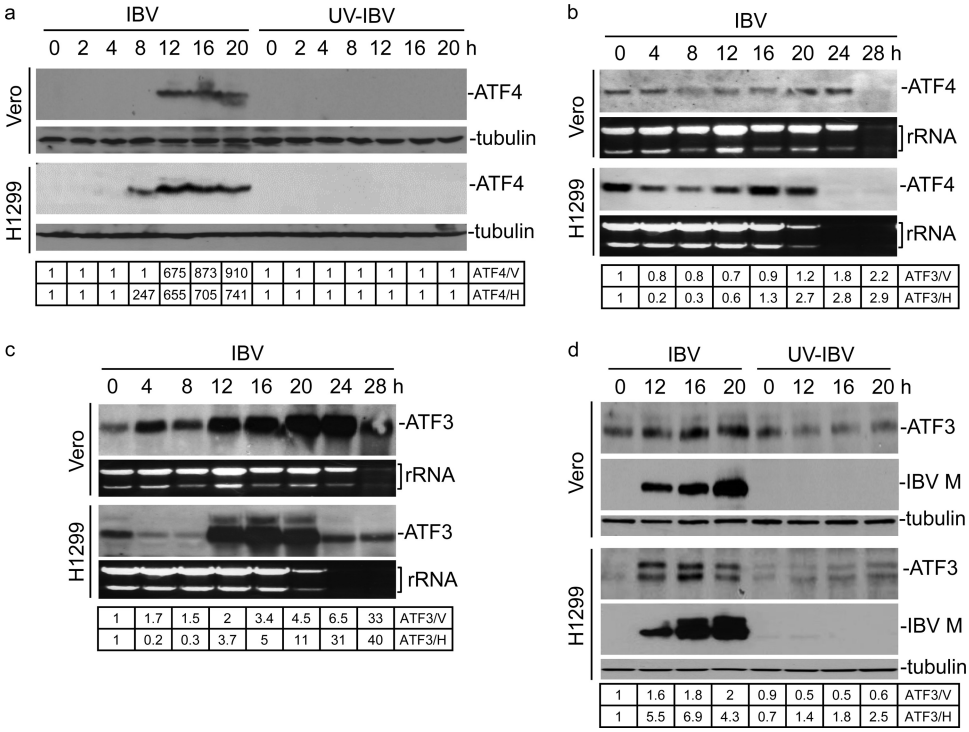

FIG 2 Induction of the PERK-eIF2α-ATF4 pathway by IBV infection. (a) ATF4 protein increases in IBV-infected cells. Vero and H1299 cells were infected with IBV (MOI of ~1) or incubated with UV-IBV and harvested at the indicated time points. Cell lysates were subjected to Western blotting using an ATF4 antibody. Tubulin was used as a loading control. Band intensities for ATF4 were determined by densitometry and normalized to those for tubulin. The tubulin intensity at 0 hpi was given a value of 1. (b) ATF4 mRNA is not induced upon IBV infection. Vero and H1299 cells were infected with IBV (MOI of ~1) and harvested at the indicated time points. Total RNA was isolated and subjected to Northern blotting using an ATF4 probe. Ethidium bromide staining of 28S rRNA and 18S rRNA is shown as a loading control. Band intensities for ATF4 were determined and normalized to those for rRNA. The rRNA intensity at 0 hpi was given a value of 1. (c) ATF3 mRNA is induced upon IBV infection. Vero and H1299 cells were infected as described for panel b. RNA extraction and Northern blotting were performed as described for panel b, using an ATF3 probe. Densitometry and quantification of ATF3 were performed as described for panel b. (d) ATF3 protein increases in IBV-infected cells. Vero and H1299 cells were infected with IBV (MOI of ~1) or incubated with UV-IBV and harvested at the indicated time points. Cell lysates were subjected to Western blotting using antibodies against ATF3 and IBV M. Tubulin was included as a loading control. Densitometry and quantification of ATF3 were performed as described for panel a. V, Vero cells; H, H1299 cells.

splicing forms of the ATF3 mRNA. Because ATF3 induction at the mRNA level coincided with the induction of ATF4 protein, it can be inferred that induction of ATF3 may be ATF4 dependent.

Induction of ATF3 at the protein level was then examined by Western blotting of Vero and H1299 cells infected with live IBV and UV-IBV. Moderate induction of ATF3 protein was observed in both Vero and H1299 cells infected with live IBV from 12 to 20 hpi (Fig. 2d). It was noted that there were two protein bands detected by the ATF3 antibody in IBV-infected H1299 cells, which may represent two different isoforms of ATF3. No induction of the protein was observed in both cell lines incubated with UV-IBV (Fig. 2d), suggesting that induction of ATF3 depends on active IBV replication. Since ATF3 is usually rapidly upregulated under various stress conditions to promote apoptosis through the regulation of downstream genes, this induction may contribute to IBV-induced apoptosis.

Induction of GADD153 and regulation of GADD153 target gene expression in IBV-infected cells. One of the proapoptotic proteins induced by ATF4 and ATF3 is GADD153, which is usually induced under prolonged ER stress (6, 9). To examine whether GADD153 expression is induced by IBV infection, analysis of GADD153 was performed at both the mRNA and protein levels. For this purpose, both Vero and H1299 cells were infected with IBV or UV-IBV and harvested at 0, 2, 4, 8, 12, 16, and 20 hpi. Total RNA was prepared and analyzed by Northern blotting. Consistent with our prediction, the transcription of GADD153 mRNA was increased from 12 to 20 hpi in both IBV-infected Vero and H1299 cells (Fig. 3a). In cells incubated with UV-IBV, no induction of GADD153 at the mRNA level was detected (Fig. 3a), confirming that the induction of GADD153 was due to active replication of IBV. At the protein level, GADD153 was barely detectable at early time points; however, its expression levels were elevated at 12 hpi and peaked at 20 hpi in IBV-infected Vero and H1299 cells (Fig. 3b), showing expression profiles similar to those for ATF4 and ATF3 induction. Again, no induction of GADD153 protein was observed in UV-IBV-infected cells (Fig. 3b).

GADD153 promotes cell death by a dual mechanism, i.e., through downregulation of antiapoptotic genes and induction of proapoptotic genes. It was reported that GADD153 suppresses antiapoptotic Bcl2 expression (11). The protective effect of Bcl2 primarily stabilizes the mitochondrial membrane potential and also prevents the release of cytochrome *c* and other apoptosis-inducing factors from mitochondria to the cytosol (27). It would be interesting to see if cellular Bcl2 protein expression was modulated by IBV infection. Western blot analysis of protein lysates showed a gradual decrease in Bcl2 expression from 12 to 20 hpi in

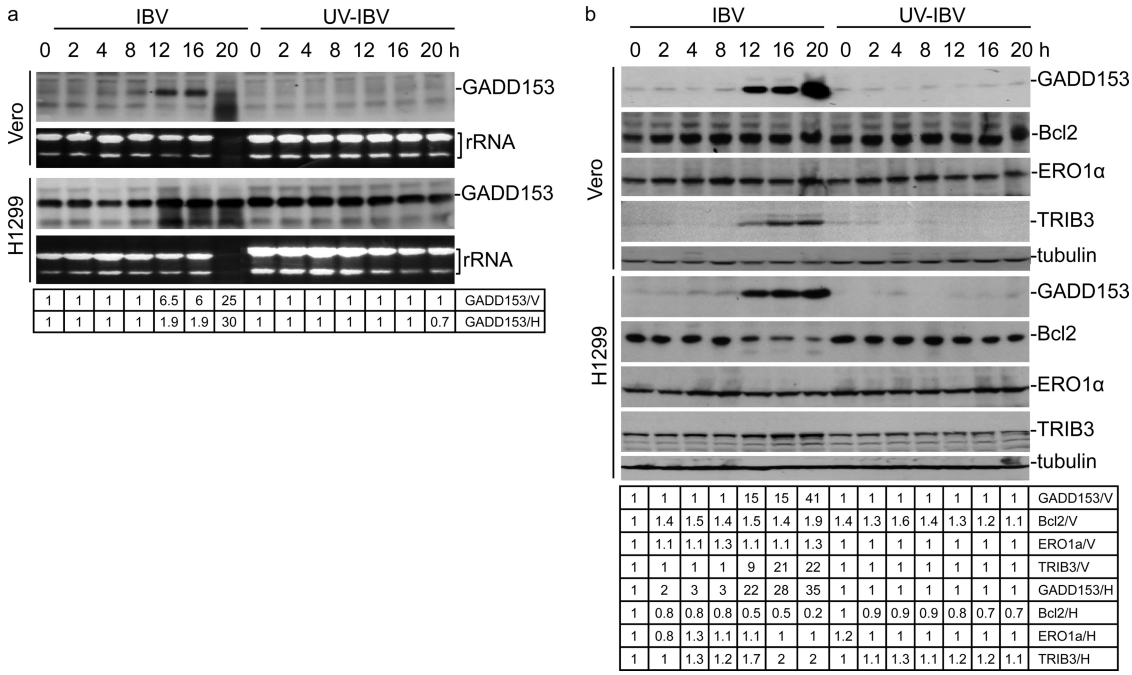

FIG 3 Induction of GADD153 and its target genes by IBV infection. (a) Induction of GADD153 at the mRNA level in IBV-infected cells. Vero and H1299 cells were infected with IBV (MOI of ~1) or incubated with UV-IBV and harvested at the indicated time points. RNA extraction and Northern blotting were performed as described in the legend to Fig. 2b, using a GADD153 probe. Densitometry and quantification of GADD153 were performed as described in the legend to Fig. 2b. (b) Induction of GADD153 and its target genes at the protein level in IBV-infected cells. Vero and H1299 cells were infected and harvested as described for panel a. Cell lysates were subjected to Western blot analysis using antibodies against GADD153, Bcl2, ERO1α, and TRIB3. Tubulin is shown as a loading control. The intensities of GADD153, Bcl2, ERO1α, and TRIB3 were determined by densitometry and normalized to that of tubulin. The tubulin intensity at 0 hpi was given a value of 1.

IBV-infected H1299 cells (Fig. 3b). However, the protein was relatively stable in IBV-infected Vero cells (Fig. 3b). This discrepancy suggests that downregulation of Bcl2 during IBV infection may be cell type specific.

Several proapoptotic proteins, including ERO1α, TRIB3, GADD34, and death receptor 5, are induced by GADD153 (9, 10, 12, 13). The expression of ERO1α, a protein that promotes cell death by enhancing cellular oxidative stress, was then examined. No increase of ERO1α expression at the protein level was observed in both IBV-infected Vero and H1299 cells (Fig. 3b), suggesting that GADD153 induction may not result in an enhancement of cellular oxidative stress in IBV-infected cells. TRIB3 is usually induced by GADD153 and could promote cell death (28). As shown in Fig. 3b, TRIB3 was significantly induced at the protein level in IBV-infected Vero cells from 12 to 20 hpi. In IBV-infected H1299 cells, the basal level of the TRIB3 protein was quite high (0 hpi), and only 1.7- to 2-fold TRIB3 induction at the protein level was observed from 12 to 20 hpi (Fig. 3b). This is consistent with a 38-fold induction of TRIB3 at the mRNA level in IBV-infected Vero cells but a mere 2-fold induction in IBV-infected H1299 cells at 16 hpi, as determined by real-time RT-PCR. It was noted that there were two bands detected by the TRIB3 antibody in the experiment with H1299 cells, which may represent isoform 1A (upper band) and isoform 1B (lower band) of TRIB3 (29, 30). TRIB3 is highly expressed in certain carcinomas, including lung, esophageal, and colonic tumors (31–34); the high basal level of TRIB3 in H1299 cells in our study further confirmed that the high expression of TRIB3 may be a common phenomenon in cancer cell lines. It is currently unknown if p53 is involved in this differential induction of TRIB3, as H1299 is a p53-null cell line. Nevertheless, the induction of TRIB3 in IBV-infected cells may help to modulate both AKT kinase and ERK activities (28, 35–37), therefore promoting apoptosis.

Involvement of PERK and PKR in GADD153 upregulation and IBV-induced apoptosis. To clarify the role of PERK in IBV-induced GADD153 upregulation, the siRNA knockdown approach was adopted. PKR was previously reported to be dephosphorylated at late stages in IBV-infected cells (25). However, it may also contribute to the phosphorylation of eIF2α at early infection stages, together with PERK. To test this possibility, knockdown of PKR was also carried out in H1299 cells. Vero cells were not chosen for knockdown experiments due to their very low transfection efficiency (data not shown). Also, Vero cells originated from African green monkeys, whose genome has not been sequenced fully. Thus, siRNA duplexes designed according to human sequences may contain mismatches, resulting in a low knockdown efficiency of the siRNAs. H1299 cells transfected with siPERK, siPKR, or a nontarget control siRNA were infected with IBV at 36 h posttransfection and harvested at 16, 18, and 20 hpi for Western blot analysis. Cleavage of PARP from the 116-kDa full-length protein [PARP(FL)] to an 85-kDa inactive polypeptide [PARP(C)] was used as a major biochemical marker of apoptosis. As shown in Fig. 4a, transfection of siPERK or siPKR significantly reduced the expression of the respective gene at the protein level compared to the level in cells transfected with the control siRNA. Significant upregulation of GADD153 was observed in IBV-infected cells transfected with the control siRNA, and much lower levels of GADD153 were observed in IBV-infected cells trans-

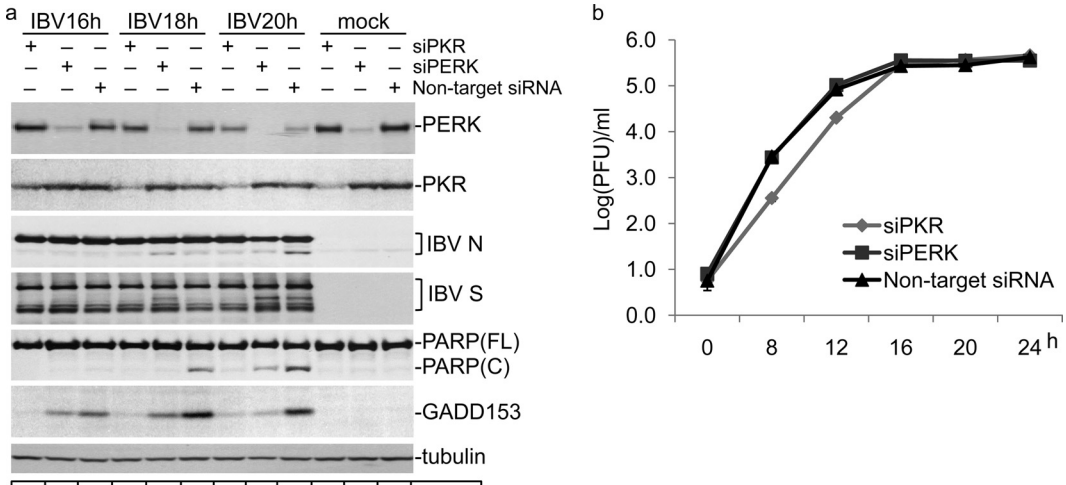

1.21	0.21	1	1.11	0.02	1	1.11	0.01	1	0.81	0.07	1	PERK
0.56	0.98	1	0.27	1.13	1	0.23	1.08	1	0.12	0.88	1	PKR
0.95	1.01	1	1.01	0.95	1	0.94	0.79	1	N.A.	N.A.	N.A.	IBV N
1.14	1.29	1	1.07	1.25	1	0.94	0.91	1	N.A.	N.A.	N.A.	IBV S
N.A.	N.A.	N.A.	0.01	0.01	1	0.01	0.25	1	N.A.	N.A.	N.A.	PARP (C)
0.04	0.45	1	0.05	0.54	1	0.07	0.21	1	N.A.	N.A.	N.A.	GADD153

FIG 4 Involvement of PERK and PKR in GADD153 induction, IBV replication, and IBV-induced apoptosis. (a) Effects of PERK knockdown and PKR knockdown on GADD153 induction, IBV replication, and IBV-induced apoptosis. H1299 cells were transfected with siPERK, siPKR, or nontarget siRNA and infected with IBV (MOI of ~2) at 36 h posttransfection. Cells were harvested at the indicated time points and subjected to Western blot analysis with antibodies against PERK, PKR, IBV N, IBV S, PARP, GADD153, and tubulin. Tubulin was used as a loading control. For PERK, PKR, IBV N, IBV S, and GADD153, band intensities were determined and normalized to that of tubulin. For PARP(C), band intensities were determined and normalized to that of PARP(FL). The intensity for cells transfected with nontarget siRNA at each time point was given a value of 1. (b) Effects of PERK knockdown and PKR knockdown on IBV replication, determined by virus titrations with culture supernatants. H1299 cells were transfected with siRNA and infected as described for panel a. At the indicated time points, culture supernatants were harvested, clarified by centrifugation, and subjected to plaque assay analysis using confluent monolayers of Vero cells. Virus titers are expressed as log PFU per ml of supernatant.

fected with either siPERK or siPKR, indicating that both PERK and PKR are involved in the activation of the eIF2α-ATF4-GADD153 pathway induced by IBV infection (Fig. 4a). Notably, the level of GADD153 was reduced to a greater extent in PKR-knockdown cells than in PERK-knockdown cells, suggesting that PKR might contribute more to the activation of the eIF2α-ATF4-GADD153 pathway. Significant cleavage of PARP was detected at 18 hpi (~19%) and 20 hpi (~30%) in the cells transfected with the control siRNA. In contrast, in cells transfected with siPERK, no PARP cleavage was detected at 16 and 18 hpi, and a significantly lower level of PARP cleavage (~12%) was observed at 20 hpi, indicating that knockdown of PERK delays and reduces IBV-induced apoptosis. In cells transfected with siPKR, PARP cleavage was barely detectable even at 20 hpi, suggesting that knockdown of PKR dramatically reduced IBV-induced apoptosis. It was noted that the patterns of PARP cleavage in PKR-knockdown cells, PERK-knockdown cells, and control cells were consistent with the levels of GADD153 expression. These results demonstrate that both PERK and PKR are involved in the IBV-induced upregulation of GADD153, which may in turn play a critical role in IBV-induced apoptosis.

The levels of two IBV structural proteins, N and S, were similar in cells transfected with siPERK, siPKR, and nontarget siRNA, indicating that deficiency in either PERK or PKR did not significantly affect IBV replication in cells (Fig. 4a). This was further supported by virus titration by plaque assay, which showed similar virus titers in the culture supernatants of cells transfected with siPKR, siPERK, or nontarget control siRNA at 16, 20, and 24 hpi (Fig. 4b). Interestingly, the virus titers for PKR-knockdown cells were lower than those for the negative-control cells at early time points (8 and 12 hpi). This may indicate that PKR has certain unidentified functions at the early stage of IBV replication.

Pharmacological intervention to inhibit the PKR-eIF2α pathway modulates IBV-induced GADD153 upregulation. To further confirm the functions of PERK and PKR in IBV-induced GADD153 upregulation, we adopted the pharmacological inhibitor approach. Unfortunately, no specific inhibitor of PERK was available at the time of this study. On the other hand, 2-AP is widely used to specifically inhibit PKR kinase activity both *in vivo* and *in vitro* (8). To investigate the role of PKR in activating the eIF2α-ATF4-GADD153 pathway, 10 mM 2-AP was added to H1299 cells at 2 hpi. Cells were harvested at 2, 8, 12, and 16 hpi and subjected to Western blot analysis. As shown in Fig. 5a, the phosphorylation of eIF2α was reduced in 2-AP-treated cells compared to that in control cells at 8 and 12 hpi, confirming that PKR contributes to the eIF2α phosphorylation at early stages in IBV-infected cells. It was noted that eIF2α phosphorylation was not suppressed by 2-AP at 16 hpi, indicating that PKR may not be the major kinase of eIF2α at this stage, possibly due to the dephosphorylation and inactivation of PKR (25). Moreover, the phosphorylation of eIF2α was not totally inhibited by 2-AP, suggesting that other kinases, such as PERK, may also contribute to eIF2α phosphorylation. Whereas GADD153 was significantly upregulated in cells treated with DMSO at 12 and 16 hpi, the level of GADD153 was suppressed to a minimal level in 2-AP-treated cells (Fig. 5a). The levels of IBV N protein were similar in 2-AP-treated cells and DMSO-treated cells; thus, the difference in GADD153 was not due to inhibition of IBV replication by 2-AP. Taken to-

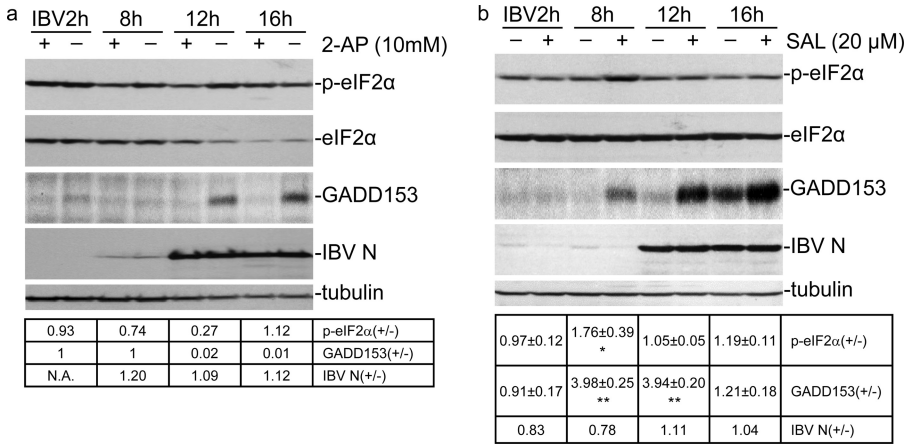

0.93	0.74	0.27	1.12	p-eIF2α(+/-)
1	1	0.02	0.01	GADD153(+/-)
N.A.	1.20	1.09	1.12	IBV N(+/-)

0.97±0.12	1.76±0.39 *	1.05±0.05	1.19±0.11	p-eIF2α(+/-)
0.91±0.17	3.98±0.25 **	3.94±0.20 **	1.21±0.18	GADD153(+/-)
0.83	0.78	1.11	1.04	IBV N(+/-)

FIG 5 Pharmacological intervention to inhibit the PKR-eIF2α pathway modulates IBV-induced GADD153 upregulation. (a) Effects of PKR activity inhibition on eIF2α phosphorylation and GADD153 induction. H1299 cells were infected with IBV (MOI of ~1) and then treated with 10 mM 2-AP or a solvent control at 2 hpi. Cells were harvested at the indicated time points and subjected to Western blot analysis with p-eIF2α, total eIF2α, GADD153, IBV N protein, and tubulin antibodies. The intensities of p-eIF2α, eIF2α, GADD153, IBV N protein, and tubulin were determined by densitometry. The ratios of the corresponding band intensities in the presence (+) and absence (−) of 2-AP were calculated and normalized (p-eIF2α ratios were normalized to the total eIF2α ratio, and GADD153 and IBV N ratios were normalized to the tubulin ratio). (b) Effects of inhibition of GADD34-PP1C activity by salubrinal (SAL) on eIF2α phosphorylation, IBV-induced GADD153 upregulation, and IBV replication. H1299 cells were infected with IBV (MOI of ~1) and treated with 20 μM SAL or a solvent control at 2 hpi. Western blotting, densitometry, and quantification were performed as described for panel a. Asterisks indicate significant differences between SAL-treated (+) and control (−) cells (*, $P < 0.05$; **, $P < 0.01$).

gether, these results confirm the role of PKR in IBV-induced eIF2α phosphorylation and GADD153 upregulation.

As reported in our previous study, IBV infection upregulates GADD34 at both the mRNA and protein levels (25). The function of GADD34 in IBV-induced activation of the eIF2α-ATF4-GADD153 pathway was further studied by addition of 20 μM salubrinal, a specific inhibitor of GADD34-PP1C activity (67), to IBV-infected H1299 cells. Addition of salubrinal inhibits PP1C activity and prevents eIF2α dephosphorylation, thereby inhibiting global translation and enhancing the expression of ATF4 and downstream targets such as GADD153. As expected, both the phosphorylated form of eIF2α and GADD153 were significantly increased in IBV-infected cells treated with salubrinal compared with DMSO-treated control cells (Fig. 5b). The levels of IBV N protein were comparable in cells treated with salubrinal and the control cells, suggesting that, at 20 μM, salubrinal did not significantly affect IBV replication. These results provide further evidence that the activated eIF2α-ATF4 pathway regulates GADD153 expression during IBV infection.

Regulation of apoptosis and IBV replication by knockdown of GADD153 through restriction of ERK activation. To clarify the role of GADD153 in IBV-induced apoptosis, knockdown of GADD153 was carried out in H1299 cells. Cells transfected with siGADD153 or nontarget control siRNA were infected with IBV at 36 h posttransfection and harvested at 16, 18, and 20 hpi. One group of cells transfected with siGADD153 or nontarget control siRNA were mock infected at 36 h posttransfection and harvested at 20 hpi as a mock infection control. The GADD153 knockdown efficiency and the effect of GADD153 knockdown on IBV replication were examined by Western blotting with antibodies against GADD153, IBV S, IBV N, and tubulin. The expression of GADD153 was efficiently knocked down (with 98% knockdown efficiency) in cells transfected with GADD153 siRNA (Fig. 6a). Both IBV S and N protein expression levels were reduced 10 to 28% in GADD153-knockdown cells at 16, 18, and 20 hpi compared to those in the control cells (Fig. 6a). These results demonstrate that virus replication is moderately suppressed in GADD153-knockdown cells, suggesting that upregulation of GADD153 during IBV infection may promote virus replication, probably through the regulation of apoptosis.

The effect of GADD153 knockdown on PARP cleavage was then analyzed. A significant amount of the PARP cleavage product was detected at 18 hpi, and was markedly increased at 20 hpi, in cells transfected with control siRNA (Fig. 6a). In contrast, much less PARP cleavage was observed in GADD153-knockdown cells at 18 and 20 hpi (Fig. 6a). These results substantiate the hypothesis that inhibition of GADD153 expression reduces IBV-induced apoptosis and that GADD153 plays a proapoptotic role in IBV-infected cells. It has previously been shown that GADD153 can upregulate TRIB3, which in turn inhibits phosphorylation of the cell survival kinase ERK1/2. The effect of GADD153 knockdown on ERK phosphorylation was thus studied. A gradual increase in p-ERK1/2 over time was observed in IBV-infected cells transfected with either GADD153 siRNA or control siRNA (Fig. 6a). However, significantly more p-ERK1/2 was detected in GADD153-knockdown cells than in control cells (Fig. 6a). These results confirmed that regulation of the ERK1/2 pathway by upregulation of GADD153 may play a functional role in modulating IBV-induced apoptosis.

To confirm that the increased phosphorylation of ERK1/2 in GADD153-knockdown cells was mediated by TRIB3, H1299 cells were transfected with TRIB3 siRNA or nontarget siRNA before being infected with IBV. As shown in Fig. 6b, the protein levels of TRIB3 were moderately reduced in cells transfected with siTRIB3 compared with those in the control cells. The level of IBV N protein was not significantly affected in TRIB3-knockdown cells, indicating that the deficiency of TRIB3 did not affect IBV replication (Fig. 6b). IBV-induced apoptosis, as determined by the cleavage of PARP, was significantly reduced in TRIB3-knockdown cells at 18 and 20 hpi compared with the negative control (Fig. 6b). Whereas the levels of total ERK1/2 remained relatively constant in both

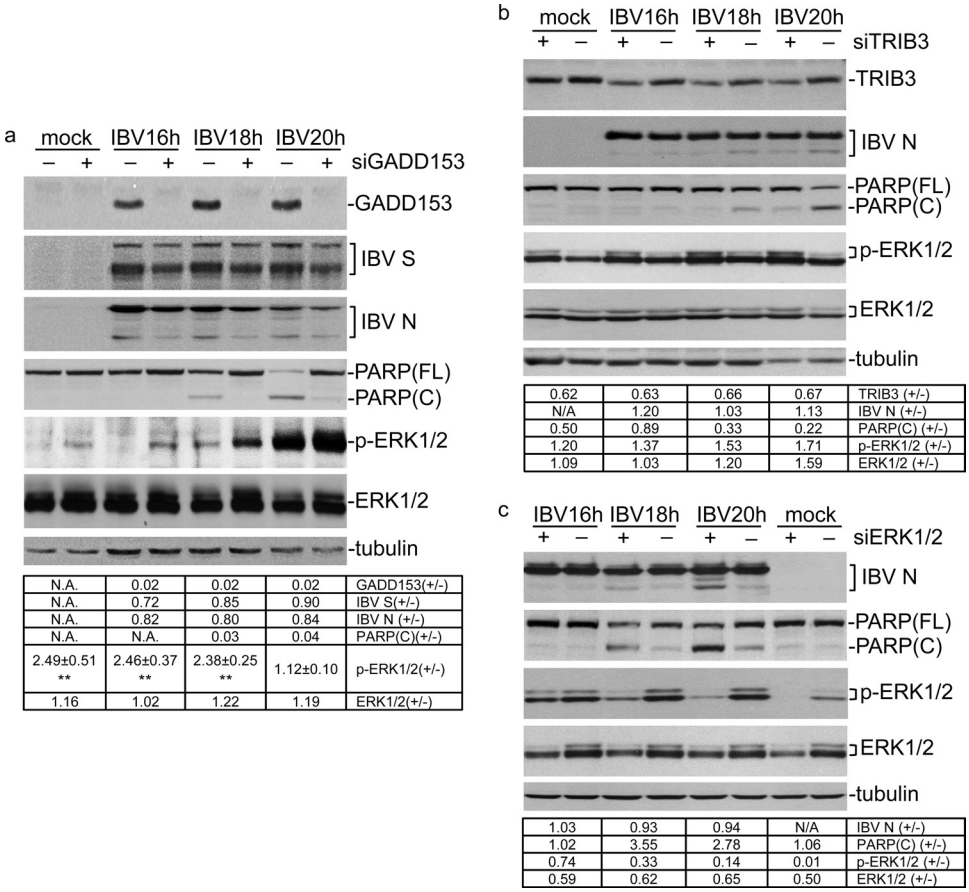

N.A.	0.02	0.02	0.02	GADD153(+/-)
N.A.	0.72	0.85	0.90	IBV S(+/-)
N.A.	0.82	0.80	0.84	IBV N (+/-)
N.A.	N.A.	0.03	0.04	PARP(C)(+/-)
2.49±0.51 **	2.46±0.37 **	2.38±0.25 **	1.12±0.10	p-ERK1/2(+/-)
1.16	1.02	1.22	1.19	ERK1/2(+/-)

0.62	0.63	0.66	0.67	TRIB3 (+/-)
N/A	1.20	1.03	1.13	IBV N (+/-)
0.50	0.89	0.33	0.22	PARP(C) (+/-)
1.20	1.37	1.53	1.71	p-ERK1/2 (+/-)
1.09	1.03	1.20	1.59	ERK1/2 (+/-)

1.03	0.93	0.94	N/A	IBV N (+/-)
1.02	3.55	2.78	1.06	PARP(C) (+/-)
0.74	0.33	0.14	0.01	p-ERK1/2 (+/-)
0.59	0.62	0.65	0.50	ERK1/2 (+/-)

FIG 6 Effects of GADD153, AKT, and ERK1/2 knockdown on IBV-induced apoptosis, upregulation of GADD153 target genes, and virus replication. (a) Effects of GADD153 knockdown on IBV replication, apoptosis, and survival kinase phosphorylation. H1299 cells were transfected with siGADD153 (+) or nontarget siRNA (−) and infected with IBV (MOI of ~2) or mock infected at 36 h posttransfection. Cells were harvested at 16, 18, and 20 hpi. The cell lysates were subjected to Western blot analysis with GADD153, IBV S and N, PARP, p-ERK1/2, and ERK1/2 antibodies. Tubulin was included as a loading control. Densitometry and quantification were performed as described in the legend to Fig. 5a. Band intensities of p-AKT and p-ERK1/2 were normalized to those of the corresponding AKT and ERK1/2 bands, respectively. Asterisks indicate significant differences between siGADD153-treated (+) and control (−) cells (**, $P < 0.01$). (b) Effects of TRIB3 knockdown on IBV replication and apoptosis. H1299 cells were transfected with siTRIB3 (+) or nontarget siRNA (−) and infected with IBV (MOI of ~2) or mock infected at 36 h posttransfection. Cell lysates were harvested and subjected to Western blotting as described for panel a, using IBV S and N, PARP, TRIB3, p-ERK1/2, and ERK1/2 antibodies. Tubulin was used as a loading control. Densitometry and quantification were done as described for panel a. (c) Effects of ERK1/2 knockdown on IBV replication and apoptosis. H1299 cells were transfected with siERK1/2 (+) or nontarget siRNA (−) and infected with IBV (MOI of ~2) or mock infected at 36 h posttransfection. Cell lysates were harvested and subjected to Western blotting as described for panel a, using IBV S and N, PARP, p-ERK1/2, and ERK1/2 antibodies. Tubulin was used as a loading control. Densitometry and quantification were performed as described for panel a.

TRIB3-knockdown and control cells, higher levels of ERK1/2 phosphorylation were detected in TRIB3-knockdown cells infected with IBV (Fig. 6b). These results indicated that TRIB3, a known effector of GADD153, negatively modulated the IBV-induced phosphorylation of ERK1/2, which may be related to the proapoptotic activity of GADD153.

The involvement of the ERK1/2 pathway in IBV-induced apoptosis was studied further by knockdown of ERK1/2 in H1299 cells by use of ERK1/2 siRNA before IBV infection. As shown in Fig. 6c, the total level of ERK1/2 was reduced by 40 to 50% in siERK1/2-transfected cells compared with the negative-control cells. Consistently, the level of phosphorylated ERK1/2 was also reduced significantly in cells transfected with siERK1/2 (Fig. 6c). The level of IBV N protein was not significantly affected in ERK1/2-knockdown cells (Fig. 6c), indicating that ERK1/2 is not essential for IBV replication. However, PARP cleavage was found to be enhanced significantly in IBV-infected ERK1/2-knockdown cells at 18 and 20 hpi compared with the negative-control cells (Fig. 6c). Taken together, these data suggest that ERK1/2 serves antiapoptotic roles during IBV infection.

DISCUSSION

Coronavirus replication and maturation are intimately associated with the host ER membrane (38, 39). It is therefore not surprising that IBV-infected cells experience ER stress. UPR is initiated to eliminate misfolded proteins and allow the infected cells to recover by attenuating translation and upregulating the expression of chaperones, degradation factors, and factors that regulate the cell's metabolic and redox environments. Some consequences of UPR, such as upregulation of chaperone expression and regulation of the metabolism and redox environments, may be beneficial to viral infection. Others, such as translational attenuation, would be deleterious. During evolution, the virus may have developed molecular devices to modulate cellular pathways for optimal in-

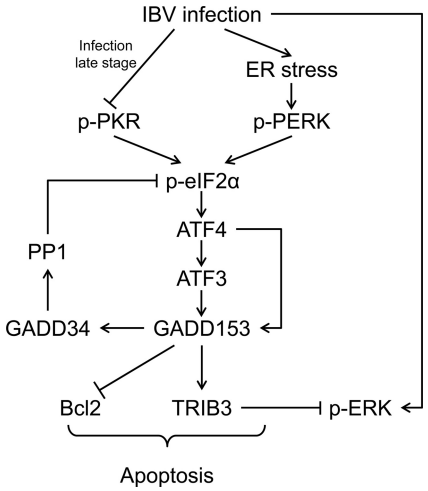

FIG 7 Working model. IBV infection causes ER stress and induces PERK phosphorylation. Phosphorylation of eIF2α by PERK and PKR induces the expression of ATF4, ATF3, and GADD153. GADD153 exerts its proapoptotic activities via suppressing Bcl2 and antagonizing the survival kinases (ERKs) by inducing TRIB3. Pointed arrows indicate activation, and blunt-ended lines indicate inhibition.

fection. In this study, we show that IBV infection activates the PERK-eIF2α-ATF4 and PKR-eIF2α-ATF4 pathways, resulting in the induction of ER stress-mediated proapoptotic pathways. This effect is achieved by inducing the proapoptotic transcription factor GADD153, which controls and suppresses the cellular survival kinase ERK1/2 (Fig. 7).

Many viruses have evolved strategies to induce ER stress and to modulate UPR. For example, human cytomegalovirus induces and modifies the UPR outcome to benefit virus replication (40), reovirus facilitates its own replication by inducing eIF2α phosphorylation and ATF4 expression (41), and rotavirus infection induces eIF2α phosphorylation but prevents the formation of stress granules to allow translation of viral mRNAs (42). More recently, severe acute respiratory syndrome coronavirus (SARS-CoV) and mouse hepatitis virus (MHV) S proteins were reported to induce ER stress and to regulate UPR for enhancement of viral replication (43, 44). MHV was also shown to modify UPR by impeding the induction of UPR-responsive genes, thereby favoring a sustained shutdown of host cell protein synthesis while enhancing translation of viral proteins (45). IBV may induce UPR through the accumulation of a large amount of viral glycoproteins in the ER. The modification of ER membrane permeability by the IBV E protein may possibly trigger ER stress as well (46–49). Moreover, during virus maturation, viral envelopes derived from the ER appear to consume the constituents of phospholipids and sterol of the ER membrane, which may activate UPR. Identification of the specific IBV proteins involved in the induction of UPR would provide insights into the mechanistic details of ER stress-mediated cell survival and apoptosis in IBV infection. However, transient expression of individual IBV proteins failed to induce UPR (data not shown). This is in contrast to data published for SARS-CoV and MHV (43, 45). Transient expression of the SARS-CoV S protein transcriptionally activated the ER chaperones GRP78 and GRP94, through PERK and eIF2α phosphorylation, and transcriptionally induced GADD153, but it had no influence on ATF4 translation (43). In MHV-infected cells, eIF2α was phosphorylated and ATF4 translation increased and resulted in translation attenuation, but induction of GADD153 and GADD34 was not observed (45). It appears that different coronaviruses may employ markedly different strategies to modulate UPR.

In this study, we showed that PERK is activated by IBV infection at early infection stages and that eIF2α is phosphorylated along with PERK activation, leading to the upregulation of ATF4, ATF3, and GADD153. Interestingly, the evidence presented demonstrates that PKR also contributed significantly to the phosphorylation of eIF2α in IBV-infected cells. IBV-induced upregulation of GADD153 was therefore achieved through activation of both the PERK-eIF2α-ATF4 and PKR-eIF2α-ATF4 pathways, which ultimately resulted in the activation of apoptotic pathways in the IBV-infected cells. It was unexpected that PKR was also actively involved in eIF2α phosphorylation in IBV-infected cells, as PKR was found to be dephosphorylated at late infection stages (25). Two possible scenarios were considered. First, a relatively high basal level of p-PKR existed in cells before infection and was detected in infected cells from 0 to 16 hpi (25), while PERK was activated only after IBV infection. The preexisting p-PKR may have played a synergistic role with IBV-activated p-PERK in the phosphorylation of eIF2α. Alternatively, the high basal level of p-PKR may have masked the detection of IBV-induced p-PKR, if a moderate level of activation occurred, in the infected cells at early infection stages. This effect would be compounded by the gradual accumulation of a virus-encoded PKR antagonist(s) if the observed dephosphorylation of PKR in IBV-infected cells at late stages of infection was mediated by such an antagonist(s) (25).

Both p-PERK and p-PKR were noted to be reduced at late infection stages. Along with the activation and inactivation of PERK and PKR, the level of p-eIF2α was increased at early infection stages and decreased at late infection stages. The dephosphorylation mechanisms of PERK and PKR at late infection stages are currently unclear but may be due to negative-feedback loops in the downstream events or to IBV-encoded dsRNA binding proteins.

Phosphorylation of eIF2α by PERK and PKR at early stages of IBV infection would be sufficient to induce the expression of ATF4, ATF3, and GADD53. The accumulation of AFT4, ATF3, and GADD153 in turn induces more target gene expression and triggers apoptosis. Similar strategies have been exploited by different families of viruses to regulate apoptosis during their replication cycles. For example, hepatitis C virus elicits UPR and triggers apoptosis through induction of GADD153 and ER calcium depletion (50–53); Tula hantavirus triggers apoptosis through the activation of caspase 12, phosphorylation of c-Jun N-terminal kinase (JNK) and c-Jun, and upregulation of GADD153 (54); Japanese encephalitis virus induces UPR and promotes cell death via activation of p38 and induction of GADD153 (55); West Nile virus induces neuronal loss by induction of GADD153 and GADD34 (56); and Borna disease virus induces apoptosis of subsets of neurons through the phosphorylation of eIF2α and induction of GADD153 (26).

The importance of GADD153 in facilitating ER stress-induced apoptosis is well documented (57), but the underlying mechanisms are not well explored. It is believed that GADD153 may induce apoptosis by overloading the ER with resurgent protein synthesis through induction of GADD34 expression, which recruits type 1 protein serine/threonine phosphatase (PP1) and dephosphorylates eIF2α, thereby relieving the translation repres-

sion, overloading the ER by recovery of protein synthesis, and accelerating cell death (58–62). GADD153 is also involved in apoptosis through promotion of oxidizing conditions in the ER by inducing ERO1α, an ER oxidase (9, 57, 63–65). The contribution of GADD153 to cell death is also coupled to the suppression of Bcl2 expression, relocation of Bax to the mitochondria, a depletion of intracellular glutathionine, and an increase in free radicals (11). TRIB3 is induced by GADD153 and may promote apoptosis by binding to the prosurvival kinase AKT, thereby preventing its phosphorylation and reducing its kinase activity (28, 35, 36). TRIB3 can also bind to mitogen-activated protein kinase kinase (MAPKK) and modulate MAPKK activity by either a positive-feed-forward or negative-feedback loop, depending on its concentration in the cells (37).

GADD34 induction in IBV-infected cells has been observed in a previous study (25). GADD34 plays an important role in IBV replication by promoting translational recovery. In this study, it was found that knockdown of GADD153 delayed IBV-induced apoptosis and slightly reduced IBV replication in H1299 cells, probably due to the impaired expression of GADD34 and decreased protein synthesis in the absence of GADD153. It was also observed that the antiapoptotic Bcl2 protein was decreased in IBV-infected H1299 cells, which may have contributed to GADD153-mediated apoptosis. In this study, TRIB3 was found to be enhanced in IBV-infected cells. More importantly, the prosurvival ERK1/2 pathways were activated in IBV-infected cells, and this activation was increased in GADD153-knockdown cells, indicating the possibility of GADD153 promoting apoptosis through inducing TRIB3 and modulating the ERK pathways. The antiapoptotic MCL1 protein was reported to be upregulated by IBV infection, and the expression level of MCL1 was also regulated by the expression level of GADD153 and activation of the ERK pathway (66). GADD153 may therefore modulate IBV-induced apoptosis by inducing the expression of GADD34, thereby recovering protein synthesis, or by inducing the expression of TRIB3, thereby suppressing the ERK pathway.

In summary, our study provides a fuller picture of the activation of the eIF2α-ATF4-GADD153 pathway and the underlying mechanisms of GADD153-induced apoptosis during IBV infection. This work reveals the proapoptotic signaling of UPR in cells infected with IBV and provides new insights into IBV-induced apoptosis.

ACKNOWLEDGMENT

This work was partially supported by a Competitive Research Programme (CRP) grant (R-154-000-529-281) from the National Research Foundation, Singapore.

REFERENCES

1. **Harding HP, Zhang Y, Ron D.** 1999. Protein translation and folding are coupled by an endoplasmic-reticulum-resident kinase. Nature **397:**271–274.
2. **Schroder M, Kaufman RJ.** 2005. The mammalian unfolded protein response. Annu. Rev. Biochem. **74:**739–789.
3. **Bertolotti A, Zhang Y, Hendershot LM, Harding HP, Ron D.** 2000. Dynamic interaction of BiP and ER stress transducers in the unfolded-protein response. Nat. Cell Biol. **2:**326–332.
4. **Haze K, Yoshida H, Yanagi H, Yura T, Mori K.** 1999. Mammalian transcription factor ATF6 is synthesized as a transmembrane protein and activated by proteolysis in response to endoplasmic reticulum stress. Mol. Biol. Cell **10:**3787–3799.
5. **Liu CY, Schroder M, Kaufman RJ.** 2000. Ligand-independent dimerization activates the stress response kinases IRE1 and PERK in the lumen of the endoplasmic reticulum. J. Biol. Chem. **275:**24881–24885.
6. **Harding HP, Novoa I, Zhang Y, Zeng H, Wek R, Schapira M, Ron D.** 2000. Regulated translation initiation controls stress-induced gene expression in mammalian cells. Mol. Cell **6:**1099–1108.
7. **Vattem KM, Wek RC.** 2004. Reinitiation involving upstream ORFs regulates ATF4 mRNA translation in mammalian cells. Proc. Natl. Acad. Sci. U. S. A. **101:**11269–11274.
8. **Jiang HY, Wek SA, McGrath BC, Lu D, Hai T, Harding HP, Wang X, Ron D, Cavener DR, Wek RC.** 2004. Activating transcription factor 3 is integral to the eukaryotic initiation factor 2 kinase stress response. Mol. Cell. Biol. **24:**1365–1377.
9. **Marciniak SJ, Yun CY, Oyadomari S, Novoa I, Zhang Y, Jungreis R, Nagata K, Harding HP, Ron D.** 2004. CHOP induces death by promoting protein synthesis and oxidation in the stressed endoplasmic reticulum. Genes Dev. **18:**3066–3077.
10. **Li G, Mongillo M, Chin KT, Harding H, Ron D, Marks AR, Tabas I.** 2009. Role of ERO1-alpha-mediated stimulation of inositol 1,4,5-triphosphate receptor activity in endoplasmic reticulum stress-induced apoptosis. J. Cell Biol. **186:**783–792.
11. **McCullough KD, Martindale JL, Klotz LO, Aw TY, Holbrook NJ.** 2001. Gadd153 sensitizes cells to endoplasmic reticulum stress by down-regulating Bcl2 and perturbing the cellular redox state. Mol. Cell. Biol. **21:**1249–1259.
12. **Ohoka N, Yoshii S, Hattori T, Onozaki K, Hayashi H.** 2005. TRB3, a novel ER stress-inducible gene, is induced via ATF4-CHOP pathway and is involved in cell death. EMBO J. **24:**1243–1255.
13. **Yamaguchi H, Wang HG.** 2004. CHOP is involved in endoplasmic reticulum stress-induced apoptosis by enhancing DR5 expression in human carcinoma cells. J. Biol. Chem. **279:**45495–45502.
14. **Young LS, Dawson CW, Eliopoulos AG.** 1997. Viruses and apoptosis. Br. Med. Bull. **53:**509–521.
15. **Gosert R, Kanjanahaluethai A, Egger D, Bienz K, Baker SC.** 2002. RNA replication of mouse hepatitis virus takes place at double-membrane vesicles. J. Virol. **76:**3697–3708.
16. **Snijder EJ, van der Meer Y, Zevenhoven-Dobbe J, Onderwater JJ, van der Meulen J, Koerten HK, Mommaas AM.** 2006. Ultrastructure and origin of membrane vesicles associated with the severe acute respiratory syndrome coronavirus replication complex. J. Virol. **80:**5927–5940.
17. **Stertz S, Reichelt M, Spiegel M, Kuri T, Martinez-Sobrido L, Garcia-Sastre A, Weber F, Kochs G.** 2007. The intracellular sites of early replication and budding of SARS-coronavirus. Virology **361:**304–315.
18. **Tooze J, Tooze SA.** 1985. Infection of AtT20 murine pituitary tumour cells by mouse hepatitis virus strain A59: virus budding is restricted to the Golgi region. Eur. J. Cell Biol. **37:**203–212.
19. **Li FQ, Tam JP, Liu DX.** 2007. Cell cycle arrest and apoptosis induced by the coronavirus infectious bronchitis virus in the absence of p53. Virology **365:**435–445.
20. **Liu C, Xu HY, Liu DX.** 2001. Induction of caspase-dependent apoptosis in cultured cells by the avian coronavirus infectious bronchitis virus. J. Virol. **75:**6402–6409.
21. **Zhong Y, Tan YW, Liu DX.** 2012. Recent progress in studies of arteriviruses- and coronavirus-host interactions. Viruses **4:**980–1010.
22. **Ng LF, Liu DX.** 1998. Identification of a 24-kDa polypeptide processed from the coronavirus infectious bronchitis virus 1a polyprotein by the 3C-like proteinase and determination of its cleavage sites. Virology **243:**388–395.
23. **Xu LH, Huang M, Fang SG, Liu DX.** 2011. Coronavirus infection induces DNA replication stress partly through interaction of its nonstructural protein 13 with the p125 subunit of DNA polymerase delta. J. Biol. Chem. **286:**39546–39559.
24. **Li FQ, Xiao H, Tam JP, Liu DX.** 2005. Sumoylation of the nucleocapsid protein of severe acute respiratory syndrome coronavirus. FEBS Lett. **579:**2387–2396.
25. **Wang X, Liao Y, Yap PL, Png KJ, Tam JP, Liu DX.** 2009. Inhibition of protein kinase R activation and upregulation of GADD34 expression play a synergistic role in facilitating coronavirus replication by maintaining de novo protein synthesis in virus-infected cells. J. Virol. **83:**12462–12472.
26. **Williams BL, Lipkin WI.** 2006. Endoplasmic reticulum stress and neurodegeneration in rats neonatally infected with borna disease virus. J. Virol. **80:**8613–8626.
27. **Adams JM, Cory S.** 1998. The Bcl-2 protein family: arbiters of cell survival. Science **281:**1322–1326.

28. **Du K, Herzig S, Kulkarni RN, Montminy M.** 2003. TRB3: a tribbles homolog that inhibits Akt/PKB activation by insulin in liver. Science **300:** 1574–1577.
29. **Hegedus Z, Czibula A, Kiss-Toth E.** 2006. Tribbles: novel regulators of cell function; evolutionary aspects. Cell. Mol. Life Sci. **63:**1632–1641.
30. **Ord D, Ord T.** 2005. Characterization of human NIPK (TRB3, SKIP3) gene activation in stressful conditions. Biochem. Biophys. Res. Commun. **330:**210–218.
31. **Bowers AJ, Scully S, Boylan JF.** 2003. SKIP3, a novel Drosophila tribbles ortholog, is overexpressed in human tumors and is regulated by hypoxia. Oncogene **22:**2823–2835.
32. **Miyoshi N, Ishii H, Mimori K, Takatsuno Y, Kim H, Hirose H, Sekimoto M, Doki Y, Mori M.** 2009. Abnormal expression of TRIB3 in colorectal cancer: a novel marker for prognosis. Br. J. Cancer **101:**1664–1670.
33. **Park MH, Cho SA, Yoo KH, Yang MH, Ahn JY, Lee HS, Lee KE, Mun YC, Cho DH, Seong CM, Park JH.** 2007. Gene expression profile related to prognosis of acute myeloid leukemia. Oncol. Rep. **18:**1395–1402.
34. **Xu J, Lv S, Qin Y, Shu F, Xu Y, Chen J, Xu BE, Sun X, Wu J.** 2007. TRB3 interacts with CtIP and is overexpressed in certain cancers. Biochim. Biophys. Acta **1770:**273–278.
35. **Bromati CR, Lellis-Santos C, Yamanaka TS, Nogueira TC, Leonelli M, Caperuto LC, Gorjao R, Leite AR, Anhe GF, Bordin S.** 2011. UPR induces transient burst of apoptosis in islets of early lactating rats through reduced AKT phosphorylation via ATF4/CHOP stimulation of TRB3 expression. Am. J. Physiol. Regul. Integr. Comp. Physiol. **300:**R92–R100.
36. **He L, Simmen FA, Mehendale HM, Ronis MJ, Badger TM.** 2006. Chronic ethanol intake impairs insulin signaling in rats by disrupting Akt association with the cell membrane. Role of TRB3 in inhibition of Akt/protein kinase B activation. J. Biol. Chem. **281:**11126–11134.
37. **Kiss-Toth E, Bagstaff SM, Sung HY, Jozsa V, Dempsey C, Caunt JC, Oxley KM, Wyllie DH, Polgar T, Harte M, O'Neill AL, Qwarnstrom EE, Dower SK.** 2004. Human tribbles, a protein family controlling mitogen-activated protein kinase cascades. J. Biol. Chem. **279:**42703–42708.
38. **de Haan CA, Rottier PJ.** 2005. Molecular interactions in the assembly of coronaviruses. Adv. Virus Res. **64:**165–230.
39. **Masters PS.** 2006. The molecular biology of coronaviruses. Adv. Virus Res. **66:**193–292.
40. **Isler JA, Skalet AH, Alwine JC.** 2005. Human cytomegalovirus infection activates and regulates the unfolded protein response. J. Virol. **79:**6890–6899.
41. **Smith JA, Schmechel SC, Raghavan A, Abelson M, Reilly C, Katze MG, Kaufman RJ, Bohjanen PR, Schiff LA.** 2006. Reovirus induces and benefits from an integrated cellular stress response. J. Virol. **80:**2019–2033.
42. **Montero H, Rojas M, Arias CF, Lopez S.** 2008. Rotavirus infection induces the phosphorylation of eIF2alpha but prevents the formation of stress granules. J. Virol. **82:**1496–1504.
43. **Chan CP, Siu KL, Chin KT, Yuen KY, Zheng B, Jin DY.** 2006. Modulation of the unfolded protein response by the severe acute respiratory syndrome coronavirus spike protein. J. Virol. **80:**9279–9287.
44. **Versteeg GA, van de Nes PS, Bredenbeek PJ, Spaan WJ.** 2007. The coronavirus spike protein induces endoplasmic reticulum stress and upregulation of intracellular chemokine mRNA concentrations. J. Virol. **81:**10981–10990.
45. **Bechill J, Chen Z, Brewer JW, Baker SC.** 2008. Coronavirus infection modulates the unfolded protein response and mediates sustained translational repression. J. Virol. **82:**4492–4501.
46. **Liao Y, Lescar J, Tam JP, Liu DX.** 2004. Expression of SARS-coronavirus envelope protein in Escherichia coli cells alters membrane permeability. Biochem. Biophys. Res. Commun. **325:**374–380.
47. **Liao Y, Yuan Q, Torres J, Tam JP, Liu DX.** 2006. Biochemical and functional characterization of the membrane association and membrane permeabilizing activity of the severe acute respiratory syndrome coronavirus envelope protein. Virology **349:**264–275.
48. **Wilson L, Gage P, Ewart G.** 2006. Hexamethylene amiloride blocks E protein ion channels and inhibits coronavirus replication. Virology **353:**294–306.
49. **Wilson L, Mckinlay C, Gage P, Ewart G.** 2004. SARS coronavirus E protein forms cation-selective ion channels. Virology **330:**322–331.
50. **Benali-Furet NL, Chami M, Houel L, De Giorgi F, Vernejoul F, Lagorce D, Buscail L, Bartenschlager R, Ichas F, Rizzuto R, Paterlini-Brechot P.** 2005. Hepatitis C virus core triggers apoptosis in liver cells by inducing ER stress and ER calcium depletion. Oncogene **24:**4921–4933.
51. **Chan SW, Egan PA.** 2005. Hepatitis C virus envelope proteins regulate CHOP via induction of the unfolded protein response. FASEB J. **19:**1510–1512.
52. **Ciccaglione AR, Costantino A, Tritarelli E, Marcantonio C, Equestre M, Marziliano N, Rapicetta M.** 2005. Activation of endoplasmic reticulum stress response by hepatitis C virus proteins. Arch. Virol. **150:**1339–1356.
53. **Ciccaglione AR, Marcantonio C, Tritarelli E, Equestre M, Vendittelli F, Costantino A, Geraci A, Rapicetta M.** 2007. Activation of the ER stress gene gadd153 by hepatitis C virus sensitizes cells to oxidant injury. Virus Res. **126:**128–138.
54. **Li XD, Lankinen H, Putkuri N, Vapalahti O, Vaheri A.** 2005. Tula hantavirus triggers pro-apoptotic signals of ER stress in Vero E6 cells. Virology **333:**180–189.
55. **Su HL, Liao CL, Lin YL.** 2002. Japanese encephalitis virus infection initiates endoplasmic reticulum stress and an unfolded protein response. J. Virol. **76:**4162–4171.
56. **Medigeshi GR, Lancaster AM, Hirsch AJ, Briese T, Lipkin WI, Defilippis V, Fruh K, Mason PW, Nikolich-Zugich J, Nelson JA.** 2007. West Nile virus infection activates the unfolded protein response, leading to CHOP induction and apoptosis. J. Virol. **81:**10849–10860.
57. **Oyadomari S, Mori M.** 2004. Roles of CHOP/GADD153 in endoplasmic reticulum stress. Cell Death Differ. **11:**381–389.
58. **Brush MH, Weiser DC, Shenolikar S.** 2003. Growth arrest and DNA damage-inducible protein GADD34 targets protein phosphatase 1 alpha to the endoplasmic reticulum and promotes dephosphorylation of the alpha subunit of eukaryotic translation initiation factor 2. Mol. Cell. Biol. **23:**1292–1303.
59. **Connor JH, Weiser DC, Li S, Hallenbeck JM, Shenolikar S.** 2001. Growth arrest and DNA damage-inducible protein GADD34 assembles a novel signaling complex containing protein phosphatase 1 and inhibitor 1. Mol. Cell. Biol. **21:**6841–6850.
60. **Ma Y, Hendershot LM.** 2003. Delineation of a negative feedback regulatory loop that controls protein translation during endoplasmic reticulum stress. J. Biol. Chem. **278:**34864–34873.
61. **Novoa I, Zeng H, Harding HP, Ron D.** 2001. Feedback inhibition of the unfolded protein response by GADD34-mediated dephosphorylation of eIF2alpha. J. Cell Biol. **153:**1011–1022.
62. **Novoa I, Zhang Y, Zeng H, Jungreis R, Harding HP, Ron D.** 2003. Stress-induced gene expression requires programmed recovery from translational repression. EMBO J. **22:**1180–1187.
63. **Matsumoto M, Minami M, Takeda K, Sakao Y, Akira S.** 1996. Ectopic expression of CHOP (GADD153) induces apoptosis in M1 myeloblastic leukemia cells. FEBS Lett. **395:**143–147.
64. **Maytin EV, Ubeda M, Lin JC, Habener JF.** 2001. Stress-inducible transcription factor CHOP/gadd153 induces apoptosis in mammalian cells via p38 kinase-dependent and -independent mechanisms. Exp. Cell Res. **267:**193–204.
65. **Wang XZ, Lawson B, Brewer JW, Zinszner H, Sanjay A, Mi LJ, Boorstein R, Kreibich G, Hendershot LM, Ron D.** 1996. Signals from the stressed endoplasmic reticulum induce C/EBP-homologous protein (CHOP/GADD153). Mol. Cell. Biol. **16:**4273–4280.
66. **Zhong Y, Liao Y, Fang S, Tam JP, Liu DX.** 2012. Up-regulation of Mcl-1 and Bak by coronavirus infection of human, avian and animal cells modulates apoptosis and viral replication. PLoS One **7:**e30191. doi:10.1371/journal.pone.0030191.
67. **Boyce M, Bryant KF, Jousse C, Long K, Harding HP, Scheuner D, Kaufman RJ, Ma D, Coen DM, Ron D, Yuan J.** 2005. A selective inhibitor of eIF2alpha dephosphorylation protects cells from ER stress. Science **307:**935–939.